**Eksakta** : Berkala Ilmiah Bidang MIPA
VOLUME 27 NO 04 2026, pp 704-718
ISSN : Print 1411-3724 — Online 2549-7464
DOI : https://doi.org/10.24036/eksakta/vol27-iss04/740

Eksakta
Berkala Ilmiah Bidang MIPA
http://www.eksakta.ppj.unp.ac.id/index.php/eksakta

*Article*

# Microwave-Synthesized Hydroxyapatite from Quail Eggshell for Pb(II) Removal

**Frisca Aulanny[1], Matlal Fajri Alif[1*], Yulia Eka Putri[1]**

[1]Department of Chemistry, Faculty of Mathematics and Natural Science, Universitas Andalas, Padang, Indonesia

**Article Info**

***Article history :***
Received July 16, 2026
Revised August 17, 2026
Accepted August 20, 2026
Published August 30, 2026
***In Press***

***Keywords :***
Quail egg shell waste,
hydroxyapatite,
Pb(II) metal ion,
microwave-assisted,
adsorption

**Abstract.** Hydroxyapatite (HAp, $Ca_{10}(PO_4)_6(OH)_2$) is a primary constituent of bones and teeth. It has also been widely developed as a promising adsorbent for removing heavy metals. In this study, Pb(II) removal was achieved via adsorption using HAp. Quail eggshell waste served as the calcium source for HAp synthesis, while $NH_4H_2PO_4$ provided the phosphate source. A microwave-assisted method was used to improve time and energy efficiency and obtain high-purity, homogeneous HAp. This study optimizes Pb(II) removal parameters using the batch adsorption method. Characterization of HAp before and after Pb(II) ion adsorption was performed using XRF, XRD, and SEM-EDX. HAp was successfully synthesized with a Ca/P molar ratio of 1.69. The study determined that optimal Pb(II) removal occurred at pH 5, with a concentration of 1100 mg/L and a contact time of 60 minutes, yielding an adsorption capacity of 499.334 mg/g and removal efficiency of 90.788%. The Langmuir isotherm model and the PSO kinetic model described the Pb(II) removal process. The material was tested on water samples from the Batang Arau River estuary, specifically near the Siti Nurbaya Bridge, achieving a removal efficiency of 89.86%. Producing HAp from quail eggshell waste using the microwave-assisted method proved effective for the adsorption of Pb(II).



***Corresponding Author :***
Matlal Fajri Alif
Department of Chemistry, Faculty of Mathematics and Natural Science,
Universitas Andalas, Padang, Indonesia
Email: mfalif@sci.unand.ac.id

## 1. Introduction

Heavy metal pollution in aquatic environments has become a major global issue with the potential to harm aquatic ecosystems and human health. Lead (Pb) is one of the heavy metals most frequently found in the environment. Lead cannot be naturally degraded, is found in relatively low concentrations, and is toxic to the human body when exposure exceeds optimal limits [1]. Based on Government Regulation No. 22 of 2021, the permissible quality standard threshold for lead (Pb) content in water bodies is 0.05 mg/L [2]. Adsorption, ion exchange, membrane filtration, and precipitation are among the many techniques developed to address high Pb levels in the environment. Because of its practical application, low operating cost, high activity, and efficiency, adsorption is thought to be the most promising method [3].

Hydroxyapatite (HAp) is a frequently used adsorbent, as it has become a key component in adsorption methods for treating hazardous water pollutants, including $Pb^{2+}$ metal ions [4]. Because of its high stability, ion-exchange capacity, environmental friendliness, low cost, and large specific surface area, HAp is often used for heavy metal removal from water [5]. The main building blocks of HAp are phosphate and calcium. Natural or artificial sources provide the calcium raw ingredients used to create HAp; fish bones, seashells, and eggshells are among the natural calcium sources [6].

The year-on-year rise in quail egg output causes a rise in quail eggshell waste. The demand for quail eggs as a protein source for the general public motivates this rise in output [7]. Direct disposal of quail eggshell waste into the environment affects visual beauty, raises trash volume, and may pose a contamination risk from environmental microbial activity [8]. One alternative use of this trash is to use its calcium content, especially calcium carbonate ($CaCO_3$), also known as calcite, which makes up 95–97% of the shell [9]. The $CaCO_3$ derived from quail eggshells can be used for the synthesis of HAp [10].

Several methods exist for HAp synthesis, including solid-state reaction, mechanochemical synthesis, solution combustion, pyrolysis, sol-gel, microemulsion, hydrothermal, and microwave-assisted synthesis [11]. Drawbacks associated with other methods include long reaction times, high chemical consumption, and the risk of introducing impurities into the final product. Additionally, Alif et al. previously employed the sol-gel method to synthesize HAp from quail eggshells for Pb(II) adsorption; however, this method has drawbacks, such as long synthesis times and the need to control pH and reaction temperature [12]. Therefore, this study uses the microwave method for HAp synthesis. Microwave-assisted synthesis is an efficient technique because it accelerates the reaction, reducing the time required compared with other methods. The application of microwave energy during thermal treatment can yield fine, homogeneous HAp with high purity [13]. The microwave method offers several advantages over other synthesis techniques, including ease of operation and environmental friendliness [6].

Furthermore, the microwave-assisted method utilizes microwave radiation to facilitate the formation of more distinct and uniform porous structures, thereby significantly enhancing the material's adsorption capacity [14]. This is because microwave radiation can accelerate HAp synthesis through direct interaction between microwave electromagnetic radiation and polar solvent molecules in the reaction medium, particularly water molecules. This interaction facilitates the absorption of radiation by polar water molecules, thereby providing sufficient energy to support rapid and homogeneous calcium phosphate nucleation and subsequent HAp crystal growth, in contrast to the slower nucleation process associated with conventional methods[15]. The rapid heating and crystallization process may also contribute to the formation of a porous structure in the synthesized HAp [16].

This study aims to synthesize HAp from quail eggshell waste using a microwave-assisted method, to evaluate HAp's capacity to adsorb Pb(II) ions as a solution to heavy metal pollution, and to analyze the characteristics of the HAp before and after adsorption with XRF, XRD, and SEM-EDX. Unlike

the earlier study, this study also implemented optimal conditions for Pb(II) adsorption by HAp, evaluated using estuarine water samples from the Batang Arau River near the Siti Nurbaya Bridge.

## 2. Experimental Section

### 2.1 Materials

The materials used in this study were commercial quail eggshells, Ammonium dihydrogen phosphate ($NH_4H_2PO_4$), nitric acid ($HNO_3$), sodium hydroxide (NaOH), lead nitrate ($Pb(NO_3)_2$), and deionized water. All chemicals used were obtained from Merck. The tools used in this study were a microwave (Multiwave 5000, Anton Paar), oven (LabTech), AAS (Shimadzu AA-7000F), furnace, analytical balance, glassware (Pyrex), blender, 200 mesh sieve (74 μm), rotary shaker (Edmund Buhler 7400 Tubingen), pH meter, hot plate and magnetic stirrer, magnetic bar, mortar and pestle, XRF (Epsilon 3XL, PANalytical), XRD (D8 Advance, Bruker), and SEM (JEOL JSM-6510).

### 2.2 Research Procedure

#### 2.2.1 Quail Eggshell Sample Preparation

Quail eggshells were washed under running water and soaked in 0.1 M $HNO_3$. The samples were then rinsed and dried. Once dry, the quail eggshells were blended into a powder [17]. Subsequently, the quail eggshell powder was sieved using a 200-mesh sieve and calcined for 5 hours at 900°C in a furnace [18].

#### 2.2.2 HAp Synthesis via the Microwave-Assisted Method

HAp was synthesized using a microwave-assisted method, employing calcined quail eggshells (CaO) as the calcium source and ammonium dihydrogen phosphate ($NH_4H_2PO_4$) as the phosphate source. Using a mortar and pestle, 4.0000 g of CaO and 4.7966 g of $NH_4H_2PO_4$ were mixed and ground, then dissolved in deionized water [14]. The mixture was stirred for 5 minutes, then placed in a microwave and heated at 200°C with an output of 1800 W and a frequency of 2.45 GHz for 5 minutes. The product of synthesis was later filtered to get a precipitate [19]. The precipitate then went into an oven to dry for three hours at 105°C [20].

#### 2.2.3 Determination of Optimum Conditions for Pb(II) Ion Adsorption by HAp

To determination of optimum condition for Pb(II) adsorption by HAp, the pH of the Pb(II) solution was changed (3, 4, 5, 6, 7, and 8), the initial Pb(II) concentration was changed (100 mg/L to 1300 mg/L), and the contact time was changed (15, 30, 45, 60, 75, and 90 minutes). In a 100 mL Erlenmeyer flask, 50 mL of Pb(II) solution was prepared. Adding 0.1 M $HNO_3$ or 0.1 M NaOH changed the solutions' starting pH. Then, every solution was mixed with 0.1 g of HAp and stirred with a shaker at 200 rpm. Finally, each solution was filtered, and the residual lead concentration in the solution was determined using AAS [12].

#### 2.2.4 Determination of Adsorption Isotherm and Kinetics Models for Pb(II) Ion Adsorption by HAp

The adsorption isotherm model for Pb(II) uptake by HAp was fitted to the Langmuir and Freundlich equations. The Langmuir isotherm equation was derived by plotting Ce versus $C_e/q_e$, while the Freundlich isotherm equation was obtained by plotting ln $q_e$ versus ln $C_e$. An $R^2$ value close to 1 indicates a suitable adsorption isotherm model. Adsorption kinetics were investigated using Pseudo-First-Order (PFO) and Pseudo-Second-Order (PSO) models, based on calculated adsorption capacities derived from contact-time variation data during HAp adsorption. The PFO kinetic equation was obtained from a plot of ln $(q_e - q_t)$ versus t, whereas the PSO kinetic equation was derived from a plot of $t/q_t$ versus t. An $R^2$ value close to 1 indicates a suitable kinetic model [21].

### 2.2.5 Application of Optimum Conditions for Pb(II) Ion Adsorption by HAp in Estuary Water Samples

The application of optimum conditions for Pb(II) adsorption by HAp was evaluated using estuary water samples from the Batang Arau River near the Siti Nurbaya Bridge. The estuary water samples were prepared in accordance with the procedures outlined in SNI 06-6989.8-2004. The initial Pb concentration of the prepared water sample was measured. The pH of the water sample was adjusted to the optimum level, then the sample was mixed with 0.1 g of HAp in a 100 mL Erlenmeyer flask. The mixture was agitated using a shaker at 200 rpm for the optimum duration. Finally, the solution was filtered, and the residual Pb concentration was measured using AAS [12].

### 2.2.6 HAp Characterization

Characterization of HAp before and after Pb(II) ion uptake was performed using XRF, XRD, and SEM-EDX to compare the characteristics of the adsorbent following the adsorption process.

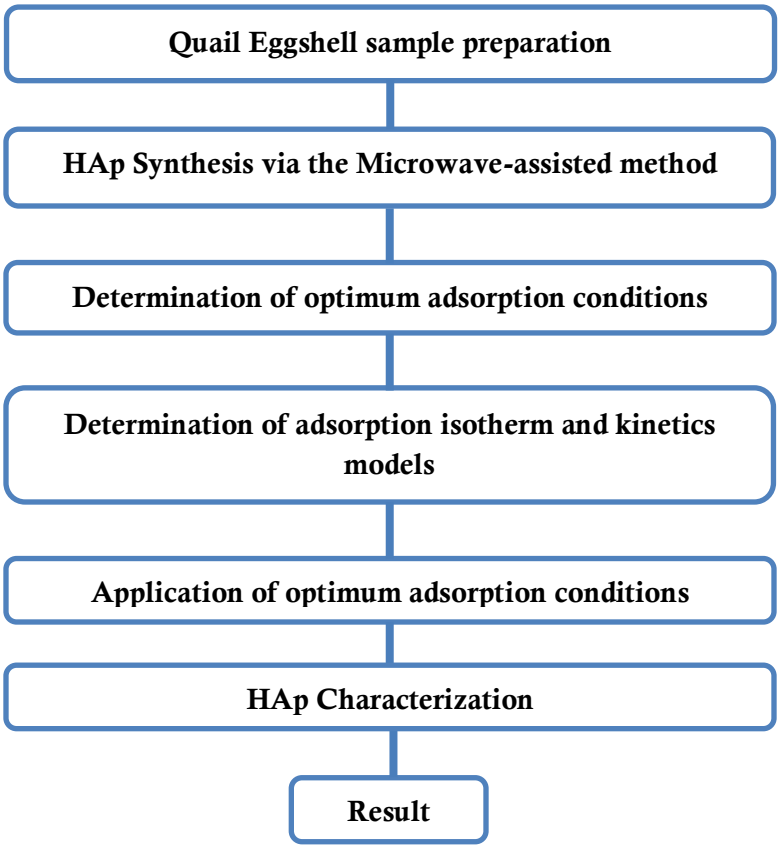


**Figure 1**. Research Flowchart

## 3. Results and Discussion

### 3.1 Analysis of Optimal Conditions for Pb(II) Ion Adsorption by HAp

pH represents a crucial factor in assessing the ability of ions to be adsorbed from water solutions. This is linked to how hydrogen ions compete with active sites on the surface of the adsorbent. The pH level can influence the charge on the adsorbent's surface as well as the extent of ionization occurring there [22].

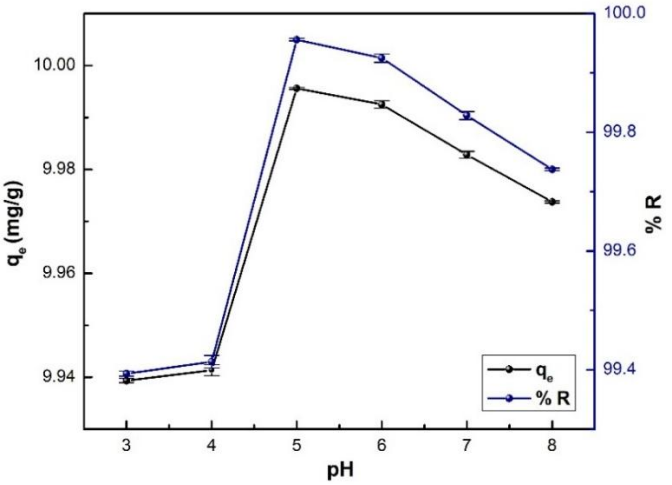


**Figure 2.** Optimum pH plot
($C_0$ = 20 mg/L; V = 50 mL; adsorbent mass = 0.1 g; t = 60 min; stirring speed = 200 rpm)

Based on Figure 2, the adsorption capacity ($q_e$) and removal efficiency (%R) values were lower at pH 3 and 4. This is attributed to competition between $H^+$ ions and Pb(II) metal ions for active sites on the HAp surface (such as $PO_4^{3-}$ and $OH^-$) [23]. At pH 5, the $q_e$ and %R values reached their optimum; thus, pH 5 is considered the optimal pH for Pb(II) ion adsorption by HAp. However, as the pH increased further to the 6–8 range, a decline in $q_e$ and %R values was observed. This is because rising pH increases the concentration of $OH^-$ ions in solution, which tend to coordinate with Pb(II) ions to form a white $Pb(OH)_2$ precipitate.

The formation of this precipitate reduces the amount of free $Pb^{2+}$ ions available to interact with the adsorbent's active sites, thereby decreasing $q_e$. The change in pH also causes several ionic forms, including $PbOH^+$, $Pb_2OH^{3+}$, $Pb(OH)_4^{2-}$, and $Pb(OH)_3^-$, to show up in the solution [24]. At alkaline or higher pH levels (pH 6–8), a significant decrease in Pb(II) metal ion concentration in the solution occurs compared to more acidic conditions; this is attributed to adsorption processes at the material's active sites and may be due to the potential formation of $Pb(OH)_2$ precipitates at higher pH values.

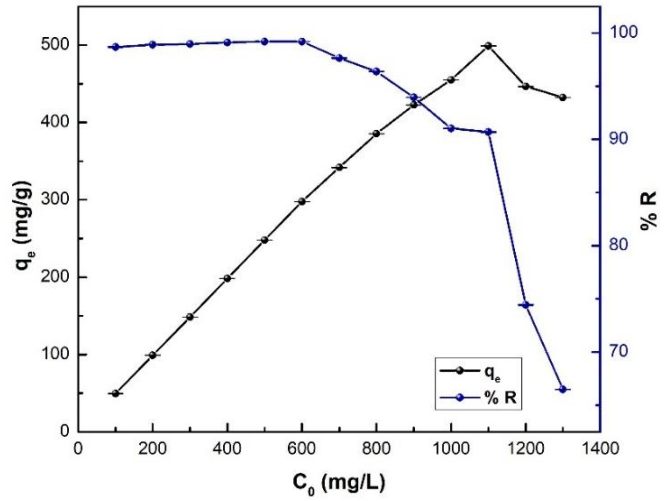


**Figure 3.** Optimum initial concentration plot
(pH = 5; V = 50 mL; adsorbent mass = 0.1 g; t = 60 min; stirring speed = 200 rpm)

According to Figure 3, the $q_e$ value rises from 100 mg/L to 1100 mg/L as the starting Pb(II) metal ion concentration ($C_0$) increases. This is mostly driven by the larger concentration gradient between the solution phase and the adsorbent surface, which serves as the primary driving force for the transfer of metal ions from the liquid phase to the solid surface. More metal ions become available to engage with the active sites on the HAp surface as the concentration of $Pb^{2+}$ ions in solution increases; this causes $q_e$ to increase [25].

However, this increase does not continue indefinitely; once the initial concentration reaches 1100 mg/L, the qe value begins to decline. This decrease shows how few active sites there are on the adsorbent surface. The mass of the adsorbent utilized is always 0.1 g; hence, there is a maximum limit on the amount of $Pb^{2+}$ ions that may be successfully adsorbed [26]. Because the active sites of the adsorbent are saturated, more Pb(II) ions remain in the solution when they are taken up by Pb(II) metal ions. This phenomenon indicates that, at that moment, adsorption has reached its saturation capacity. Thus, the percentage removal (%R) of HAp decreases with increasing initial Pb(II) concentration ($C_0$). This happens because, at excessive concentrations, the amount of $Pb^{2+}$ ions in the solution surpasses the capacity of the accessible active sites; the adsorbent surface saturates and is no longer able to bind the remaining metal ions, thereby lowering the %R automatically [27].

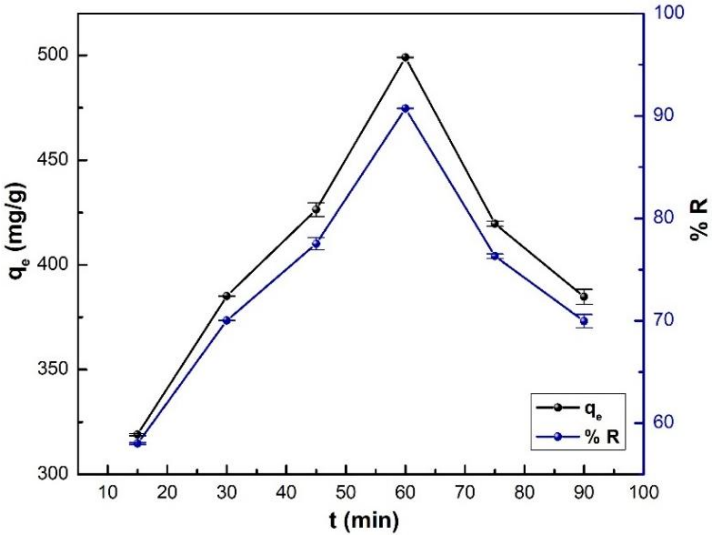


**Figure 4.** Contact time plot
(pH = 5; V = 50 mL; $C_0$ = 1100 mg/L; adsorbent mass = 0.1 g; stirring speed = 200 rpm)

One factor influencing adsorption capacity, among others, is contact time. The rate of reaction, that is, how quickly a species' concentration varies with time, is connected to contact time. The contact time is used to get the best stirring time during the batch process such that the adsorbent can absorb metal ions to the greatest degree. The longer the contact time, the more adsorbate is adsorbed. Long contact times enable greater adsorption of adsorbate molecules and diffusion [28]. The values of $q_e$ and %R rose notably during the 15–60 minutes contact time range, as seen in Figure 4. The high $C_0$ of Pb(II) metal ions in the solution causes this phenomenon since it increased the frequency of successful collisions between the Pb(II) ions and the active sites on the adsorbent surface. Therefore, the absorption of Pb(II) ions was quick, as many active sites were still accessible and readily available for the Pb(II) ions.

However, the values of $q_e$ and %R began to decline once the optimal contact time of 60 minutes was reached. This may indicate the establishment of a dynamic adsorption-desorption equilibrium after 60 minutes. This behavior suggests that the surface sites have become saturated and the adsorption rate has decreased due to the limited availability of active sites. Furthermore, partial

desorption or redistribution of Pb(II) metal ions on the adsorbent surface may occur, contributing to the observed decrease in adsorption capacity [29].

**Table 1.** Pb adsorption capacity results of HAp using different Ca precursors and synthesis methods

| Ca source | HAp synthesis method | $q_e$ (mg/g) | Reference |
|---|---|---|---|
| Golden apple snail shell | Sol-gel | 123.460 | [20] |
| Chicken eggshell | Precipitation | 129.100 | [30] |
| Chicken eggshell | Hydrothermal | 94.300 | [31] |
| Beef bone | Calcination | 152.600 | [32] |
| Quail eggshell | Sol-gel | 285.930 | [12] |
| Quail eggshell | Microwave-assisted | 499.334 | This study |

The results of the comparison with other HAp samples are presented in Table 1. Based on the data regarding optimum pH, optimum concentration, and optimum contact time for Pb(II) ion adsorption by HAp obtained from previous results, the optimum conditions for Pb(II) adsorption by HAp were determined. The adsorption capacity of 499.334 mg/g achieved by HAp in this study demonstrates that the microwave method is not only time- and energy-efficient but also effective in producing HAp with a notably high adsorption capacity compared to other synthesis methods and calcium precursors.

### 3.2 Analysis of Isotherm and Kinetics Models for Pb(II) Ion Adsorption by Hap

Figure 5 and Table 2 show the correlation coefficient ($R^2$) values for the Langmuir and Freundlich isotherms. Based on the $R^2$ values, it can be concluded that the adsorption by HAp follows the Langmuir isotherm model; the $R^2$ value of 0.9981, close to 1, indicates that the Langmuir model is highly suitable for describing the adsorption of Pb(II) metal ions by HAp. The Langmuir model assumes that the uptake of Pb(II) metal ions occurs on the homogeneous surface of HAp via monolayer adsorption and involves uniform adsorption [31]. Langmuir model suggests that certain active sites on the adsorbent surface scale with its surface area [33].

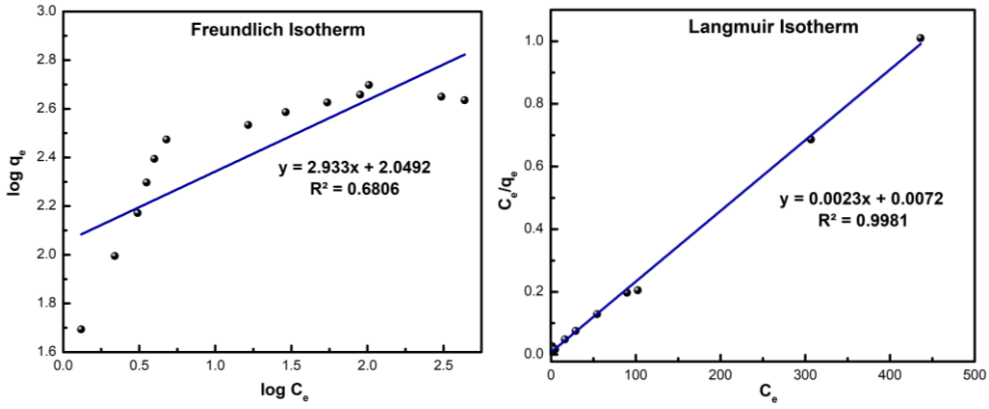


**Figure 5.** Adsorption isotherm graph (Freundlich and Langmuir)

**Table 2.** Isotherm model parameters for Pb(II) Ion Adsorption by HAp

| Isotherm model | Equation | Parameters | Result |
|---|---|---|---|
| Langmuir | $q_e = \frac{q_m K_L C_e}{1+K_L C_e}$ | $q_m$ (mg $g^{-1}$) | 434.7826 |
| | | $K_L$ (L $mg^{-1}$) | 1.0000 |
| | | $R^2$ | 0.9981 |
| Freundlich | $q_e = K_F C_e^{1/n}$ | $K_F$ | 0.0128 |
| | | n | 0.4309 |
| | | $R^2$ | 0.6806 |

Figure 6 shows the linear plot of t versus $\ln(q_e–q_t)$ for the PFO model and the linear plot of t versus $t/q_t$ for the PSO model.

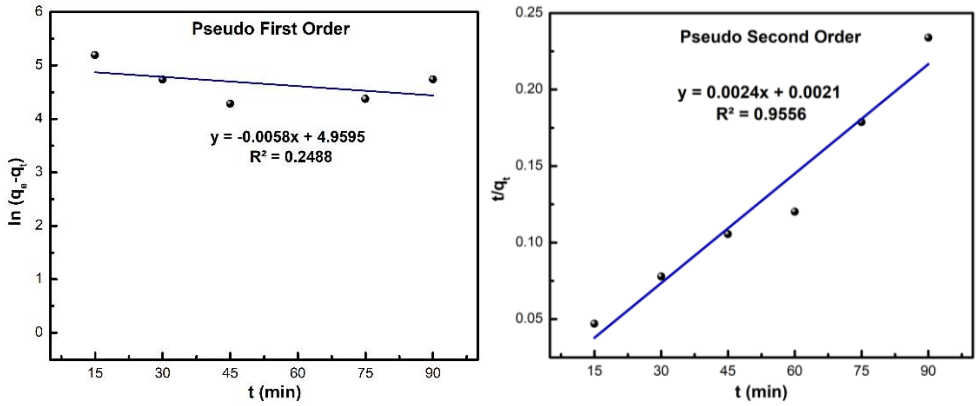


**Figure 6.** Adsorption kinetics graph (PFO and PSO)

Table 3 shows that the $R^2$ value for the PSO model is closer to 1 than that of the PFO model. This indicates that Pb(II) adsorption by HAp follows the PSO kinetic model, implying that chemisorption is the dominant mechanism. In fact, the chemisorption process confirms the involvement of surface functional groups ($OH^-$, $PO_4^{3-}$) on HAp [29].

**Table 3.** Kinetic model parameters for Pb(II) Ion Adsorption by HAp

| Kinetic model | Equation | Parameters | Result |
|---|---|---|---|
| Pseudo First Order | $\ln(q_e-q_t) = \ln q_e - k_1 t$ | $K_1$ ($min^{-1}$) | 0.0134 |
| | | $q_e$ calc (mg $g^{-1}$) | 142.5225 |
| | | $R^2$ | 0.2488 |
| Pseudo Second Order | $\frac{t}{q_t} = \frac{1}{k_2 q_e^2} + \frac{t}{q_e}$ | $K_2$ (mg $g^{-1}min^{-1}$) | 0.0027 |
| | | $q_e$ calc (mg $g^{-1}$) | 416.6670 |
| | | $R^2$ | 0.9556 |

### 3.3 Results of Applying Optimum Conditions for Pb(II) Adsorption by HAp to Water Samples

The selection of this location was based on various scientific considerations and environmental aspects. Notably, the site is strategically positioned to receive runoff and discharges from diverse human activities, including vessel traffic, tourism, and domestic waste disposal, as well as potential impacts from industrial waste along the riverbanks. The accumulation of waste from these various sources can lead to elevated levels of heavy metals, such as Pb(II), in the estuarine waters. Furthermore, the area holds significant ecological and social value, making water quality monitoring there crucial.

Consequently, tests were conducted using HAp as an eco-friendly adsorbent to reduce heavy metal contamination; the material was tested directly on river water from the site to evaluate its effectiveness under real-world conditions. The optimal conditions employed in these tests were a pH of 5 and a contact time of 60 minutes. The initial Pb(II) ion concentration ($C_0$) in the water sample was 0.8628 mg/L, while the concentration after the adsorption process ($C_e$) decreased to 0.0875 mg/L. Based on the difference between $C_0$ and Ce, the Pb(II) removal efficiency of the HAp adsorbent was calculated and reported in the final column as %R (removal), yielding 89.86%. This result demonstrates that HAp possesses very high efficiency in adsorbing Pb(II) ions from contaminated river water, even under actual environmental conditions. The results of applying these optimal conditions to the estuarine water sample are presented in Table 4 below.

**Table 4.** Results of applying optimum conditions for Pb(II) metal adsorption by HAp to water samples

| | pH | Contact time | $C_o$ (mg/L) | $C_e$ (mg/L) | %R |
|---|---|---|---|---|---|
| **Pb(II)** | 5 | 60 min | 0.8628 | 0.0875 | 89.86% |

### 3.4 Analysis of HAp Characterization

XRF analysis was conducted before and after Pb(II) uptake to compare the chemical composition of HAp and to determine whether Pb(II) metal ions had been successfully adsorbed. Table 7 presents the XRF analysis results before Pb(II) uptake, revealing the presence of CaO and $P_2O_5$, the primary components of HAp, with a Ca/P molar ratio of 1.69; this value closely approximates the theoretical ratio of 1.67 for stoichiometric HAp, a material characterized by high stability and insolubility [34]. Although the ideal value was not reached, the ratio indicates that the HAp structure was well formed. Following Pb(II) uptake, a decrease in CaO and $P_2O_5$ content was observed, alongside the appearance of PbO (65.067%) in the HAp. These findings confirm that Pb(II) uptake by HAp occurred and that an ion exchange between $Ca^{2+}$ and $Pb^{2+}$ took place [35].

**Table 4.** XRF results of HAp before and after Pb(II) adsorption

| Component (Oxide) | Composition (%) | |
|---|---|---|
| | Before adsorption | After adsorption |
| CaO | 62.728 | 16.999 |
| $P_2O_5$ | 37.116 | 17.206 |
| PbO | - | 65.067 |
| Ca/P ratio | 1.69 | |

Based on Figure 7, the XRD pattern of HAp synthesized from quail eggshell waste matches the standard HAp pattern (ICDD 00-009-0432), corresponding to a hexagonal HAp structure [36]. The alignment of the peak positions with the standard indicates that the HAp was successfully synthesized. The characteristic peaks of HAp appear at 2θ values of 25.8°, 31.8°, 32.2°, 32.9°, 34.1°, 39.8°, 46.7°, and 49.5°, corresponding to the HAp crystal planes (002), (211), (112), (300), (202), (130), (222), and (213) [37]. Additionally, an impurity in the form of aragonite ($CaCO_3$) appears in the HAp at a 2θ angle of 24°.

After adsorption, new peaks emerged, indicating the formation of new phases when compared against the standard patterns of two reference compounds: Hydroxypyromorphite ($Pb_{10}(PO_4)_6(OH)_2$) (ICDD 01-087-2477) and Lead Phosphate ($Pb_3(PO_4)_2$) (ICDD 00-025-1394). This demonstrates that the XRD pattern observed after Pb(II) ion adsorption matches the diffraction patterns of these standards [38]. These results indicate that a reaction occurred between Pb(II) ions and the phosphate groups in HAp resulting in the formation of more stable new compounds, such as Hydroxypyromorphite and Lead Phosphate [39].

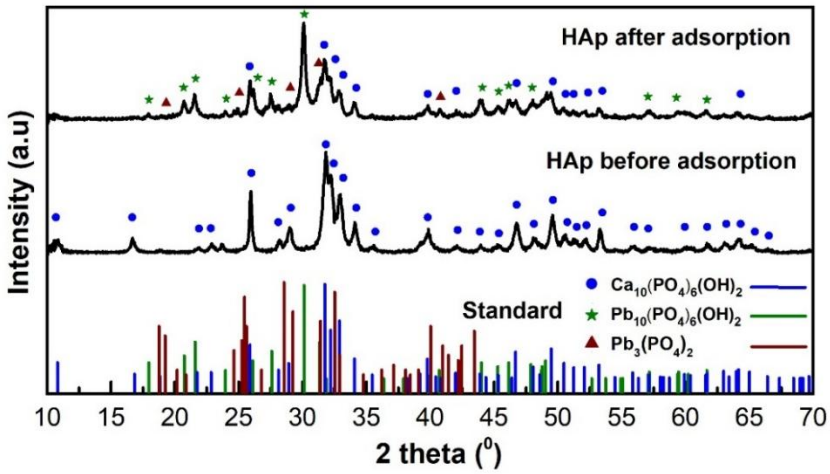


**Figure 7.** XRD diffraction pattern before and after adsorption

In addition to the emergence of a new phase, several characteristic HAp peaks exhibited a slight decrease in intensity following adsorption. This reduction in intensity reinforces the indication that $Pb^{2+}$ ions undergo an ion exchange mechanism with $Ca^{2+}$ ions within the HAp structure. This substitution occurs because metal ions have a strong affinity for functional groups on the HAp surface, such as hydroxyl and phosphate groups. The ion exchange results in lattice parameter defects because the ionic radius of $Pb^{2+}$ (±1.19 Å) is larger than that of $Ca^{2+}$ (±1.00 Å) [40]. The occurrence of this ion exchange mechanism aligns with the adsorption data fitted to the Langmuir isotherm model; this indicates that the ion exchange between $Pb^{2+}$ ions and $Ca^{2+}$ cations in the HAp structure proceeds stoichiometrically at homogeneous active sites (monolayer), where each site specifically binds a single ion without interactions between the adsorbed molecules.

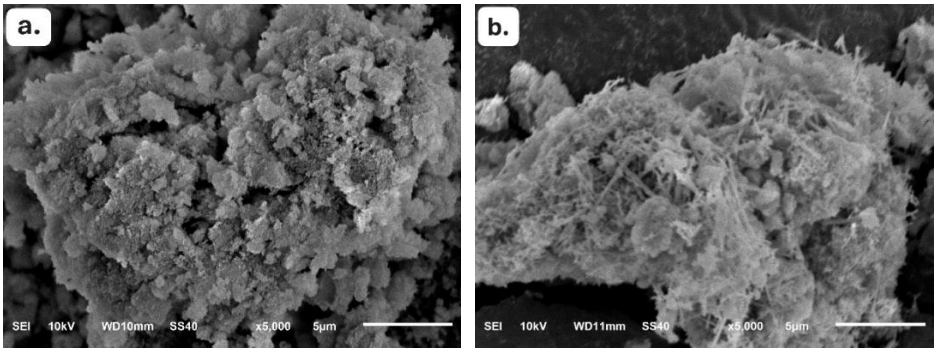


**Figure 8.** SEM micrograph of HAp: a. before adsorption and b. after adsorption.

Figure 8 a shows that the morphology of HAp synthesized via the microwave-assisted method consists of small, irregularly shaped particles with a strong tendency toward agglomeration or aggregation. This phenomenon is driven by high surface reactivity and surface energy, alongside van der Waals forces and hydrogen bonding between HAp particles [41]. In SEM analysis, this agglomeration manifests as the formation of massive structures and dense, bulky multi-layered aggregates [42]. Such aggregation has significant negative consequences, including poor dispersion in water, a drastic reduction in specific surface area, and the blocking of active binding sites, which ultimately limit the HAp's adsorption performance regarding pollutants [43].

Figure 8 b. shows the micrograph of HAp after Pb(II) ion adsorption, revealing a drastic change in surface morphology. The HAp surface appears rougher and irregular, forming new aggregates with fibrous or needle-like structures; this indicates an interaction between Pb(II) ions and the surfaces of HAp [44]. This is most likely attributable to the ionic substitution of $Ca^{2+}$ by $Pb^{2+}$ within the HAp lattice or the formation of a new, stable, and insoluble compound, such as hydroxylpyromorphite.

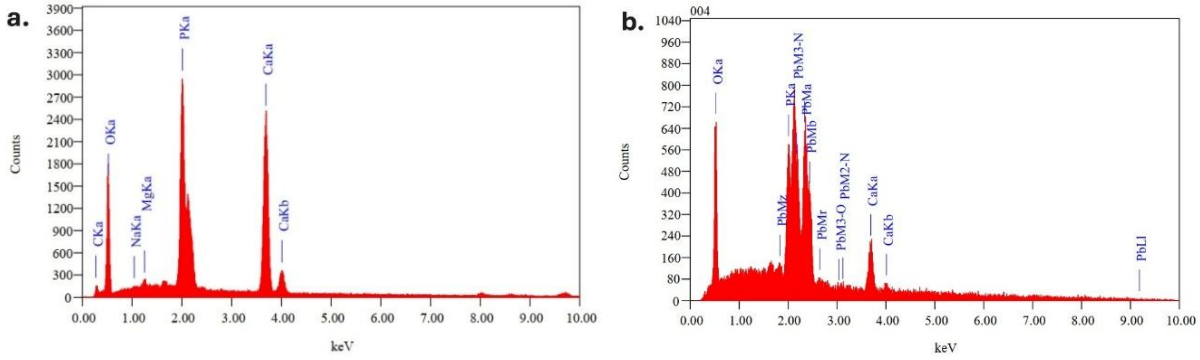


**Figure 9.** EDX spectrum of HAp: a. before adsorption and b. after adsorption

EDX analysis serves to determine the elemental composition of a specific surface, complementing the SEM micrograph results [42]. Figure 9 a shows that point 'a' exhibits a surface morphology consisting of irregularly shaped particle agglomerates; this result is supported by the EDX spectrum, which detected the primary elements oxygen (O), phosphorus (P), and calcium (Ca), the main constituents of HAp. The relatively high peak intensities of Ca and P indicate the successful formation of the HAp phase [45]. The EDX spectrum after adsorption of Pb(II) ions on Figure 9 b still displays characteristic HAp peaks, such as those for Ca, P, and O. Additionally, signal peaks corresponding to Pb elements, including Pb Mα and Pb Mβ, appear, confirming the successful adsorption of $Pb^{2+}$ ions onto the HAp surface. The presence of Pb peaks in the EDX spectrum indicates that the adsorption process proceeded effectively [46].

## 4. Conclusion

Based on the research conducted, hydroxyapatite (HAp) was successfully synthesized from quail eggshells using a microwave-assisted method and utilized as an adsorbent for Pb(II) metal ions. Adsorption tests revealed that the synthesized HAp possessed high adsorption capability, achieving a removal efficiency of 90.788% and a maximum adsorption capacity of 499.334 mg/g under optimal conditions (pH 5, initial concentration of 1100 mg/L, and contact time of 60 minutes). The adsorption process followed the Langmuir isotherm model, indicating monolayer adsorption on a homogeneous surface, and Pseudo-Second-Order (PSO) kinetics, suggesting a chemisorption mechanism. Furthermore, the HAp was successfully applied to real wastewater samples from the Batang Arau River estuary (specifically near the Siti Nurbaya Bridge), achieving a removal efficiency of 89.86%. Thus, HAp derived from quail eggshells demonstrates significant potential as an eco-friendly adsorbent for removing heavy metal Pb(II) ions from aquatic environments.

## 5. Acknowledgement

This research was funded by the Directorate of Research, Technology, and Community Service, Directorate General of Higher Education, Research, and Technology, Ministry of Education, Culture, Research, and Technology of the Republic of Indonesia, under the Fundamental Research – Regular Scheme (Research Contract Number: 041/E5/PG.02.00.PL/2024 for the 2024 Fiscal Year).

## References

[1] Mitra, S., Chakraborty, A.J., Tareq, A.M., Emran, T., Nainu, F., Khusro, A., Idris, A.M., Khandaker, M.U., Osman, H., Alhumaydhi, F.A., Simal-Gandara, J. (2022). Impact of heavy metals on the environment and human health: Novel therapeutic insights to counter the toxicity. *Journal of King Saud University - Science*, *34*(3).

[2] Wardana, M.T. dan Kuntjoro, S. (2023). Analisis Kadar Logam Berat Timbal (Pb) di Perairan Pelabuhan Teluk Lamong dan Korelasinya terhadap Kadar Pb pada Kerang Darah (Tegillarca granosa). *LenteraBio : Berkala Ilmiah Biologi*, *12*(1), 41–49.

[3] A. Hamid, Z. Rahmawati, M. Abdullah, T. E. Purbaningtyas, F. Rohmah, and I. D. Febriana. (2022). The Influence of NaOH Activator Concentration on the Synthesis of Activated Carbon from Banana Peel for Pb(II) Adsorption. *Eksakta*, *23*(03), 158–166.

[4] El Hammari, L., Hamed, R., Azzaoui, K., Jodeh, S., Latifi, S., Saoiabi, S., Boukra, O., Krime, A., Boukra, A., Saoiabi, A., Hammouti, B., Khan, M.M., Sabbahi, R., Hanbali, G., Berisha, A., Taleb, M., Dagdag, O. (2023). Optimization of the adsorption of lead(II) by hydroxyapatite using a factorial design: Density functional theory and molecular dynamics. *Frontiers in Environmental Science*, *11*(March), 1–17.

[5] Jaffar, F.H., Othman, M.H.D., Ismail, N.J., Puteh, M.H., Kurniawan, T. A., Abu Bakar, S., Abdullah, H. (2024). Hydroxyapatite-based materials for adsorption, and adsorptive membrane process for heavy metal removal from wastewater: Recent progress, bottleneck and opportunities. *Journal of the Taiwan Institute of Chemical Engineers*, *164*.

[6] Goh, K.W., Wong, Y.H., Ramesh, S., Chandran, H., Krishnasamy, S., Sidhu, A., Teng, W.D. (2021). Effect of pH on the properties of eggshell-derived hydroxyapatite bioceramic synthesized by wet chemical method assisted by microwave irradiation. *Ceramics International*, *47*(7), 8879–8887.

[7] Malau, N.D. (2021). Manufacture And Characterization Of Hydroxyapatite From Quail Eggshell Using Precipitation Methods. *International Journal of Progressive Sciences and Technologies (IJPSAT*, *29*(1), 484–490.

[8] D. Yonata, S. Yonata, S. Aminah, and W. Hersoelistyorini. (2017). Kadar Kalsium dan Karakteristik Fisik Tepung Cangkang Telur Unggas dengan Perendaman Berbagai Pelarut," *J. Pangan dan Gizi*, *7*(2), 82–93,

[9] A. Razak, N. M. Isa, and S. Adzila. (2021). Synthesis of calcium phosphate extracted from eggshell waste through precipitation method. *Biointerface Res. Appl. Chem.*, *11*(6), 15058–15067.
[10] Vinayagam, R., Kandati, S., Murugesan, G., Goveas, L.C., Baliga, A., Pai, S., Varadavenkatesan, T., Kaviyarasu, K., Selvaraj, R. (2023). Bioinspiration synthesis of hydroxyapatite nanoparticles using eggshells as a calcium source: Evaluation of Congo red dye adsorption potential. *Journal of Materials Research and Technology*, *22*, 169–180.
[11] Castro, M.A.M., Portela, T.O., Correa, G.S., Oliveira, M.M., Rangel, J.H.G., Rodrigues, S.F., Mercury, J.M.R. (2022). Synthesis of hydroxyapatite by hydrothermal and microwave irradiation methods from biogenic calcium source varying pH and synthesis time. *Boletín de la Sociedad Española de Cerámica y Vidrio*, *61*(1), 35–41.
[12] Alif, M.F., Darajat, S., dan Azizah, S. (2024). Utilization of Hydroxyapatite from Quail Eggshells as an Adsorbent for Lead. *Indonesian Journal of Environmental Management and Sustainability*, *9*(2025), 20-27.
[13] S. A. Perwiranegara, Athanasius Priharyoto Bayuseno, and Rifky Ismail. (2021). Pengaruh Daya Microwave Terhadap Karakterisasi Hidroksiapatit Berbahan Cangkang Rajungan. *J. Tek. Mesin S-1*, *9*(4), 1–6.
[14] J. Jiang, Y. Long, X. Hu, J. Hu, M. Zhu, and S. Zhou. (2020). A facile microwave-assisted synthesis of mesoporous hydroxyapatite as an efficient adsorbent for $Pb^{2+}$ adsorption. *J. Solid State Chem.*, *289*(April), 121491,
[15] Heakal, F.E.T., Sarhan, Y.B., Maamoun, M.A., Bakry, A.M., Abdel-Monem, Y.K., Ghayad, I.M. (2022). Hydrothermal Microwave-Assisted Fabrication of Nanohydroxyapatite Powder and Optimization of Its Nanocomposite Coatings on Magnesium Alloy for Orthopedic Applications. *ACS Omega*, *7*(1), 1021–1034.
[16] Karunakaran, G., Suresh, G., Cho, E., Sunwoo, Y., Kolesnikov, E., Kuznetsov, D. (2019). Microwave-assisted hydrothermal synthesis of mesoporous carbonated hydroxyapatite with tunable nanoscale characteristics for biomedical applications. *Ceram. Int.*, *45*(September 2018), pp. 970–977.
[17] Gowri, A. and Kala, K. (2022) 'Evaluating synthesis of Novel Hydroxyapatite from Egg Shell Compared with Chemically Synthesized HAp for Orthopedic application', *Journal of Pharmaceutical Negative Results*, 13(4).
[18] Alif, M.F., Fitria, R.A., Arief, S., Triandini, S., Manawan, M., Purnama, P., Goei, R. (2024). Peat water purification using nanohydroxyapatite synthesized from Carbon Negative Precipitated Calcium Carbonate precursor. *Sustainable Chemistry for the Environment*, *6*, 100105.
[19] Amalia, T.R., Nurlely, dan Sari, Y.W. (2020). Synthesis of Hydroxyapatite Using Microwave Irradiation and Sintering with Variation pH and Time. *Journal of Physics: Conference Series*, *1505*(1).
[20] Hariani, P.L., Said, M., dan Salni (2019). Effect of sintering on the mechanical properties of hydroxyapatite from fish bone (Pangasius Hypophthalmus). *IOP Conference Series: Materials Science and Engineering*, *509*(1).
[21] Dhamala Shobita C., Ahmad Fadli, K. (2020). Model Kesetimbangan Pada Adsorpsi Ion Logam Timbal ($Pb^{2+}$) Menggunakan Hidroksiapatit. *7*, 1–5.
[22] I. Lestari, S. Devi, E. Putri, M. Asti, and D. R. Gusti. (2022). Adsorption of Mercury from Aqueous Solution on Durian ( Durio zibethinus ) Seed-Immobilized Alginate. *Eksakta*, *23*(01), 30–41.
[23] L. Qin, Y. Wu, Z. Hou, and E. Jiang. (2020). Influence of biomass components, temperature and pressure on the pyrolysis behavior and biochar properties of pine nut shells. *Bioresour. Technol.*, 313, 123682.
[24] Mahmud, M., Hossain, S., Mobarak, M., Quddus, S., Bashar, Muhammad S., Akhtar, U.S., Jahan, S.A., Islam, D., Ahmed, S. (2022). Engineering GO@Zn–Hap@CA porous

heterostructure for ultra-fast and ultra-high adsorption efficacy: investigation towards the remediation of chromium and lead. *Environmental Science: Advances*, *1*(5), 827–848.

[25] M. N. Hassan, M. M. Mahmoud, A. A. El-Fattah, and S. Kandil. (2016). Microwave-assisted preparation of Nano-hydroxyapatite for bone substitutes. *Ceram. Int.*, *42*(3), 3725–3744.

[26] H. I. Adegoke, F. A. Adekola, I. T. Olowookere, and A. L. Yaqub. (2017). Thermodynamic studies on adsorption of lead (II) Ion from aqueous solution using magnetite, activated carbon, and composites. *J. Appl. Sci. Environ. Manag.*, *21*(3), 440.

[27] Yang, W., Lu, C., Liang, B., Yin, C., Lei, G., Wang, B., Zhou, X., Zhen, J., Quan, S., Jing, Y. (2023). Removal of Pb(II) from Aqueous Solution and Adsorption Kinetics of Corn Stalk Biochar. *Separations*, 10.

[28] I. Lestari, Y. Ramadhanty, L. Marlinda, and Ngatijo. (2021). Preparation and Characterization of Magnetite $Fe_3O_4$ - Activated Carbon Composite as Adsorbent Cr(VI) Ion. *Eksakta*, *22*(04), 238–247.

[29] F. Waarsyat, Desy K., Sri B.E., Trisna K.S., Saddam H., Jeningsih, Septian B. (2026). Biosorption of Indigo Carmine onto Duck Egg White-Modified Longan Peel Biosorbent: Effect of Particle Size and Contact Time. *Eksakta*, vol. *27*(02), 155–166.

[30] Bernalte, E., Kamieniak, J., Randviir, E.P., Bernalte-García, Á. (2019). The preparation of hydroxyapatite from unrefined calcite residues and its application for lead removal from aqueous solutions. *RSC Advances*, *9*(7), 4054–4062.

[31] Shi, D., Tong, H., Lv, M., Luo, D., Wang, P., Xu, X., Han, Z. (2021). Optimization of hydrothermal synthesis of hydroxyapatite from chicken eggshell waste for effective adsorption of aqueous Pb(II). *Environmental Science and Pollution Research*, *28*(41), pp. 58189–58205.

[32] Ramdani, A., Kadeche, A., Adjdir, M., Taleb, Z., Ikhou, D., Taleb, S., Deratani, A. (2020). Lead and cadmium removal by adsorption process using hydroxyapatite porous materials. *Water Practice and Technology*, *15*(1), 130–141.

[33] D. Kurniawati, I. Lestari, F. Tarmizi, N. L. Pernadi, and A. Iqbal. (2023). Biosorption of Methylene Orange Dye using Langsat Shell by Batch Method. *Eksakta*, *24*(03), 305–314.

[34] Imran, E., Mei, M.L., Li, K.C., Ratnayake, J., Ekambaram, M., Cooper, P.R. (2024). Dental Applications of Ion-Substituted Hydroxyapatite: A Review of the Literature. *Dentistry Journal*, *12*(10).

[35] Zein, R., Deswati, D., Fauzia, S., Pisya, N.F. (2024). Comparative study of Pb(II) and Cr(VI) removal using Cassava peel (Manihot Esculenta Crantz). *International Journal of Phytoremediation*, *0*(0), 1–10.

[36] González-Gonzáleza, B.G., García-Sifuentes, C.O., Santacruz-Ortega, H., Brown-Bojórqueza, F., Navarro-Gautrína, R.E., Sugich-Miranda, R., Carvajal-Milláand, E. (2023). Properties of hydroxyapatite from tilapia (Oreochromis niloticus) bones: An approach towards its potential use as a dye adsorbent. *Journal of Applied Research and Technology*, *21*, 447–456.

[37] Kawsar, M., Hossain, S., Bahadur, N.M., Islam, D., Ahmed, S. (2025). Crystalline structure modification of hydroxyapatite via a hydrothermal method using different modifiers. *Materials Advances*, *6*, 3889–3902.

[38] Zhu, Y., Zhu, Z., Zhao, X., Liang, Y., Huang, Y. (2015). Characterization, dissolution, and solubility of lead hydroxypyromorphite $[Pb_5(PO_4)_3OH]$ at 25-45°C. *Journal of Chemistry*.

[39] Wipada, C., Rittirong J., Tongpak D., Sudawadee Y., Rungsan C., Ekkachai K. (2025). Microwave - assisted hydrothermal synthesis of hydroxyapatite from fermented fish by - product for removal of lead from contaminated water. *Basic Appl. Sci.*, *14*(116), 1–22.

[40] Arogundade, I., Hefnawy, M., Ofudje, E.A., El Gamal, A., Emran, T.B. (2025). Pb and Cd removal from aqueous solutions onto calcium-phosphate hydroxyl surface : kinetics, isotherms and thermodynamic investigations. *Journal of Taibah University for Science*, *19*.

[41] Zhang, Q., Lu, L., Liang, M., Wang, D., Huang, D., Zhu, Y. (2022). Efficient Treatment of Lead-containing Wastewater Using Bagasse Biochar Modified via Hydroxylapatite. *BioResources, 17*(1), 1205–1231.
[42] Wang, C., Luo, M., Xie, C., Li, K., Hang, F., Shi, C., Doherty, W.O.S. (2022). Effective Adsorption of Colorants from Sugarcane Juice by Bagasse-Based Biochar-Hydroxyapatite Composite. *Foods*, *11*, 1–19.
[43] Kim, H.J., Han, J.W., Yu, J.H., Kwak, J., Son, C., Jun, B.M., Chon, K. (2025). Hydroxyapatite and magnetic hydroxyapatite biochar from pine nut husks for anionic azo dye adsorption : Performance and reusability assessment. *Applied Surface Science*, *707*.
[44] Saisa-Ard, O., Somphon, W., Dungkaew, W., Haller, K.J. (2014). Evidence of a lead metathesis product from calcium hydroxyapatite dissolution in lead nitrate solution. *Advances in Materials Science and Engineering*, 1–7.
[45] Ali, D.A., Saad, F.A., and Elsawy, H.A. (2025). Kinetics and Isotherm Studies for Adsorption of Gentian Violet Dye from Aqueous Solutions Using Synthesized Hydroxyapatite. *Journal of Environmental and Public Health, 2023.*
[46] Iconaru, S.L., Motelica-Heino, M., Guegan, R., Beuran, M., Costescu, A., Predoi, D. (2018). Adsorption of Pb(II) ions onto hydroxyapatite nanopowders in aqueous solutions. *Materials*, *11*.